LIMNOLOGY
and
OCEANOGRAPHY

ASLO

Limnol. Oceanogr. 64, 2019, 1627–1640

doi: 10.1002/lno.11140

Resource limitation determines temperature response of unicellular plankton communities

Camila Serra-Pompei ,[1]* **George I. Hagstrom,**[2] **André W. Visser,**[1] **Ken H. Andersen**[1]

[1]Centre for Ocean Life, National Institute of Aquatic Resources (DTU-Aqua), Technical University of Denmark, Kongens Lyngby, Denmark

[2]Department of Ecology and Evolutionary Biology, Princeton University, Princeton, New Jersey

Abstract

A warmer ocean will change plankton physiological rates, alter plankton community composition, and in turn affect ecosystem functions, such as primary production, recycling, and carbon export. To predict how temperature changes affect plankton community dynamics and function, we developed a mechanistic trait-based model of unicellular plankton (auto-hetero-mixotrophic protists and bacteria). Temperature dependencies are specifically implemented on cellular process rather than at the species level. As the uptake of resources and metabolic processes have different temperature dependencies, changes in the thermal environment will favor organisms with different investments in processes such as photosynthesis and biosynthesis. The precise level of investments, however, is conditional on the limiting process and is ultimately determined dynamically by competition and predation within the emergent community of the water column. We show how an increase in temperature can intensify nutrient limitation by altering organisms' interactions, and reduce relative cell-size in the community. Further, we anticipate that a combination of temperature and resource limitation reduces ecosystem efficiency at capturing carbon due to strengthening of the microbial loop. By explicitly representing the effects of temperature on traits responsible for growth, we demonstrate how changes on the individual level can be scaled up to trends at the ecosystem level, helping to discern direct from indirect effects of temperature on natural plankton communities.

Climate change is expected to alter the functioning of marine microbial communities and associated ecosystem processes, such as primary production, trophic transfer to higher trophic levels (HTLs), and carbon sequestration. The impacts occur through changes in the physical environment and through the direct effect of temperature on physiological processes within the cell. Until recently, the focus has been on how changes in the physical environment alter the resource availability for plankton (Doney 2006). For example, rising global temperatures can lead to a stronger stratification of the water column, limiting the mixing of nutrients into the photic zone (Behrenfeld et al. 2006). Conversely, sea ice thawing can increase light availability, triggering blooms earlier in the year and prolonging its duration (Kahru et al. 2011). Taken together, the changes in ecosystem function are the result of a delicate balance between positive and negative effects driven by changes in the physical environment.

Despite temperature being the key component of global change, attention has only recently turned to the direct effects of temperature on individual plankton cells and associated ecosystem processes (Allen et al. 2005; López-Urrutia and Morán 2007; Toseland et al. 2013; Edwards et al. 2016; Sommer et al. 2017; Thomas et al. 2017). Temperature affects most metabolic processes by accelerating enzyme activity (Eppley 1972; Raven and Geider 1988). Cellular processes such as biosynthetic and respiration rates tend to double with a temperature increase of 10°C ($Q_{10} \approx 2$), also leading to an increase of the maximum potential growth rate with temperature with a $Q_{10} \approx 2$ (Eppley 1972). Yet, in nature, growth tends to be restricted not only by metabolic functions but also by the availability of resources (Clarke 2003; Marañón et al. 2018; Morán et al. 2018). Therefore, the temperature dependence of resource uptake rates also matters (Shuter 1979). For example, the affinity for light (slope of the photosynthetic rate at low light levels) is fairly insensitive to temperature, and mainly depends on the concentration of chlorophyll and chloroplasts (Raven and Geider 1988). Hence, in light-limited environments, growth will be almost independent of temperature. Uptake of dissolved compounds, e.g., nutrients or dissolved organic matter (DOM), is limited by the diffusive rate (Munk and Riley 1952; Kiørboe 2008); therefore, the response to temperature in nutrient-limited environments would be controlled by the scaling of diffusivity, which is weak, and not

*Correspondence: mcsp@aqua.dtu.dk

by enzymatic activity. Taken together, the temperature response of a cell could vary between being neutral (no change) to varying a factor 2 over a 10°C change, depending upon whether growth is limited by light, resource uptake, or biosynthesis.

However, the response of a community not only depends on the cellular-level response but also on how the community composition changes. Species have adapted their physiology to maximize growth in a given environment, resulting in a left skewed unimodal curve (reaction norm), which peaks at the optimal temperature (Thomas et al. 2012). This curve has been shown to vary according to the level of resources (Thomas et al. 2017), due to a balance between protein investments into various functions, with a steep drop at high temperature as increasing investment in chaperones to assist protein folding limits growth (Chen and Laws 2017). Conversely, species are able to modify their optimal temperature through adaptations, where an increase in the photosynthetic capacity of cells has been observed in warmer conditions (Schaum et al. 2017). The community response to a temperature change emerges when the curves from all species are added. Therefore, when a resource is limiting, the growth rate of the overall community might stay the same, but the community composition can change due to the different temperature optima of each species (*see* Edwards et al. [2016], for a good example). Therefore, an understanding of the community level temperature responses must account for the changes in the community composition, as new winners can emerge under changed temperature conditions (Dutkiewicz et al. 2013).

To assess how the direct effects of temperature alter the fitness of individual cells, and potentially scale to ecosystem processes, we developed a trait-based model of the plankton community. A cell is described by two traits: its size and its investments in phototrophy vs. biomass synthesis (biosynthesis). All processes in the model are affected by temperature: light harvesting, resource uptake, predation, and metabolism; however, the emergent population-level temperature response depends on which processes are limiting. The trait-based formulation makes it possible to reduce model complexity dramatically while at the same time resolving the adaptive nature of the plankton community under changing temperatures. We use the model to address the question of how community structure and function changes with temperature. We focus on three central aspects of ecosystem function: primary production (the amount of carbon fixed), carbon flow towards HTLs, and export to depth and dissolved pathways (such as refractory DOM [rDOM]). The exploration is done by embedding the cell-model into a physical one-dimensional (1D) water column model.

Methods

We consider a minimal food-web model of marine unicellular organisms that represents heterotrophic bacteria and mixotrophic flagellates and/or ciliates. The cell model is later embedded in a planktonic biogeochemical food-web framework. In the following, we first describe the biological compartments (generalists and bacteria), then the temperature scaling of vital rates, and finally the planktonic food web and the coupling to the physical environment.

Generalists

The cell model has a simple physiology which captures the main processes for uptake of resources, biosynthetic rate, and respiration. How temperature affects each process is introduced further down. A cell can acquire carbon by phototrophy, nitrogen by diffusive uptake, and a mix of nitrogen and carbon by phagotrophy (Fig. 1). Cells have three functional compartments: photosynthetic machinery, biosynthetic machinery, and structural material, into which the cell invests various proportions of its carbon mass. The photosynthetic mass (e.g., chloroplasts and pigments) fixes carbon. Biosynthetic mass (e.g., mitochondria and ribosomes) converts fixed carbon to functional cellular material. Finally, structural mass is associated with those structures essential for the cell integrity, such as cell walls and membranes, but that are not directly responsible for cell growth. It is assumed that cells do not have a storage compartment, such that they grow directly in pace with the uptake of resources and the activity of the biosynthetic apparatus. Finally, for simplicity, cells have a fixed C : N ratio.

Total mass of the cell V (μg C cell^{-1}) is divided among structural mass, photosynthetic machinery $\varphi_L V$ (μg C cell^{-1}), and biosynthetic machinery $\varphi_B V$ (μg C cell^{-1}). We assume that cells invest half of the acquired mass on structure, and the rest of acquired mass can be invested either in the photosynthetic or biosynthetic apparatus (Fig. 1), with the consequent tradeoff that $\varphi_L + \varphi_B = 1/2$. Hence, total mass of a cell becomes $V = V(\varphi_L + \varphi_B + 1/2)$, allowing the resource uptake strategy of a cell to be described by a single trait, $\varphi_L = \varphi_B - 1/2$.

Uptake rates of resources—light, nutrients, and food—and biosynthesis are represented by Monod kinetics (Monod 1949). Carbon fixation J_L (μg C d^{-1}) inside a cell is

$$J_L = M \frac{A_L L}{A_L L + M} \quad (1)$$

where L is irradiance (W m^{-2}), A_L is affinity for light (μg C d^{-1} [W m^{-2}]$^{-1}$), which depends on the investments, and M is the maximum biosynthetic rate (μg C d^{-1} cell^{-1}). All fluxes J are per cell, and thus given in units of μg C d^{-1} cell^{-1}.

The affinity for light absorption depends on the investment in the photosynthetic apparatus φ_L. However, absorption is also limited by the cell surface area, proportional to $V^{2/3}$. Considering both effects, the affinity for light becomes (Chakraborty et al. 2017)

$$A_L = c_L V^{2/3} \frac{a_L \varphi_L V}{a_L \varphi_L V + c_L V^{2/3}} \quad (2)$$

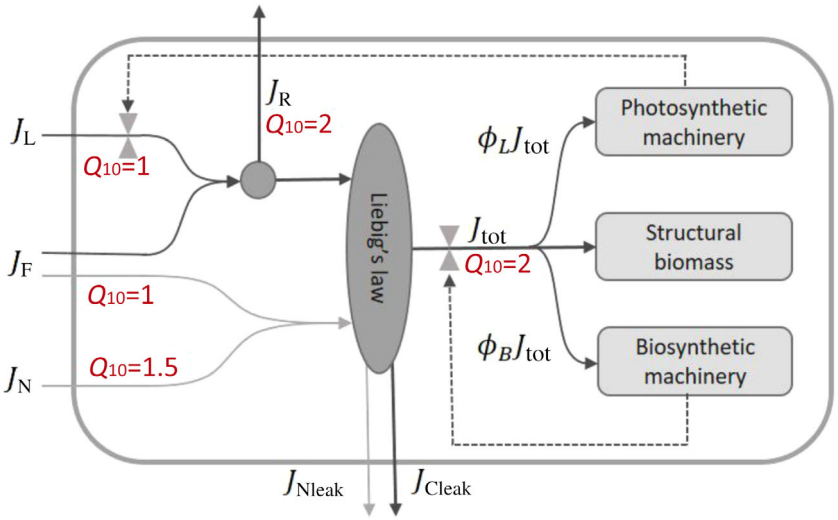

Fig. 1. Schematic representation of the generalist cell model. Total mass of the cell (V) is divided in three compartments: structural mass ($\frac{1}{2}V$), photosynthetic machinery ($\varphi_L V$), and biosynthetic machinery ($\varphi_B V$). Acquired carbon from photosynthesis (J_L), nitrogen from diffusive uptake (J_N), and carbon and nitrogen from food (J_F) are synthesized in the biosynthetic apparatus following Liebig's law of the minimum. Newly produced biomass is then allocated to either the photosynthetic apparatus, the biosynthetic apparatus, or to structural biomass according to the partitioning of investments in photosynthesis (φ_L) and biosynthesis (φ_B) (hourglass symbols show the positive feed-backs of these allocations). Part of the cellular carbon is respired (J_R). Excess N or C resulting from Liebig's minimum is excreted back to the environments (J_{Nleak} and J_{Cleak}, respectively). [Color figure can be viewed at wileyonlinelibrary.com]

where c_L is the maximum photosynthetic affinity (μg C d^{-1} [W m^{-2}]$^{-1}$), and a_L the affinity per investment in photosynthesis (μg C d^{-1} [W m^{-2}]$^{-1}$ [μg C$^{2/3}$]$^{-1}$). At very high investments or under optimal light levels, the affinity is dominated by the first term of the right-hand side, i.e., proportional to $V^{2/3}$, whereas at low investment, the affinity is proportional to cell volume V.

Nitrogen uptake (J_N) by a cell is

$$J_N = M\frac{Q_{C:N}A_N N}{Q_{C:N}A_N N + M} \tag{3}$$

where N is dissolved nitrogen (μg N L^{-1}), and A_N nitrogen affinity (L d^{-1} cell^{-1}). J_N is in units of carbon, whereas N in nitrogen; the conversion is implemented through the fixed C : N ratio $Q_{C:N}$ (μg C μg N^{-1}). Nutrient uptake is considered diffusion limited, scaling with the radius of the cell rather than by the surface area (Munk and Riley 1952). Hence, affinity for nutrients becomes

$$A_N = \alpha_N V^{1/3} \tag{4}$$

where α_N is nutrient affinity per biomass (L d^{-1} [μg C$^{1/3}$]$^{-1}$).

Food uptake J_F, that is, consumption of prey with concentration F (μg C L^{-1}) is

$$J_F = M\frac{A_F F}{A_F F + M} \tag{5}$$

In the model, a large generalist (G_2) can eat a smaller generalist (G_1), which at its turn, G_1 can predate on bacteria (B).

The clearance rate of active prey encounter scales in average linearly with cell volume (Kiørboe 2011), and so affinity A_F (L d^{-1} cell^{-1}) is

$$A_F = \alpha_F V \tag{6}$$

where α_F is the specific affinity for food (L d^{-1} [μg C]$^{-1}$).

The maximum uptake rate of each process is determined by the maximum biomass synthesis rate, which is proportional to the mass of the biosynthetic apparatus.

$$M = \mu_{max}\varphi_B V \tag{7}$$

where μ_{max} is the specific maximum biosynthesis rate per investment (d^{-1}).

Respiration rate associated with cell maintenance are assumed to be the same for all machinery, and approximately scale with body mass (Kiørboe and Hirst 2014).

$$J_R = kV \tag{8}$$

where k is the maintenance cost (d^{-1}).

As growth requires both carbon and nutrients, Liebig's law of the minimum is applied. The total carbon flux is then:

$$J_{tot} = \min[J_L + J_F - J_R,\ J_N + J_F] \tag{9}$$

Note that the nutrient flux is measured in units of carbon through the assumption of a fixed C : N ratio, which is implemented in Eq. 3. Finally, the carbon-specific population division rate μ (d^{-1}) is defined by the increase in mass.

Table 1. Variables and parameters.

Parameter	Description	Units	Value	Q_{10}
G_1, G_2, B	Concentration of G_1, G_2, and B in the system	μg C L^{-1}		
V_B	Cell mass of B	μg C cell^{-1}	10^{-8}	
V_1	Cell mass of G_1	μg C cell^{-1}	10^{-5}	
V_2	Cell mass of G_2	μg C cell^{-1}	10^{-2}	
φ_L	Investment in photosynthesis	—		
φ_B	Investment in biosynthesis	—		
a_L	Affinity per investment in photosynthesis	μg C d^{-1} (W m^{-2})$^{-1}$ μg C^{-1}	0.21	1
c_L	Maximum light affinity	μg C d^{-1} (W m^{-2})$^{-1}$ (μg C$^{2/3}$)$^{-1}$	0.005	1
α_N	Nutrient affinity	L d^{-1} (μg C$^{1/3}$)$^{-1}$	3.7×10^{-5}	1.5
α_F	Food affinity	L d^{-1} (μg C)$^{-1}$	0.005	1
α_{DOC}	Affinity for DOC	L μg C^{-1} d^{-1}	8.8×10^{-6}	1.5
K_{POM}	Half saturation constant for POM hydrolysis	μg C L^{-1}	80	
μ_{POM}	Maximum POM hydrolysis rate	μg C d^{-1} cell^{-1}	4×10^{-8}	2
μ_{max}	Maximum specific growth rate	d^{-1}	2	2
k	Metabolic cost	d^{-1}	0.05	2
$Q_{C:N}$	C : N ratio	μg C μg N^{-1}	5.68	
δ	Fraction of dead matter going to N and DOM	—	0.3	
γ	Background mortality	L (μg C d)$^{-1}$	0.02	
m_{HTL}	Loss rate to predation of HTL	d^{-1}	0.03	2
N	Nutrients concentration	μg N L^{-1}		
L	Irradiance	W m^{-2}		
D	DOC concentration	μg C L^{-1}		
P	POM concentration	μg C L^{-1}		
F	Food: concentration of prey perceived by a predator	μg C L^{-1}		

All parameters were obtained from the literature. Parameters of generalist except for biosynthetic rate come from Chakraborty et al. (2017), who obtained those by inferring from observations. Note that in Chakraborty et al. (2017), they use structural biomass and we use total biomass, so all the parameters that are multiplied by the structural biomass have here been divided by 2 (considering our assumption of structural biomass being half the total biomass). Affinity for light was derived from Daines et al. (2014). Parameters from generalists that could be extended to bacteria by allometric laws were maintained (affinity for nitrogen [αN] and maximum growth rate). Affinity for DOC was derived from Thingstad et al. (2007). Degradation rates of POM from bacteria were obtained from Anderson and Williams (1998). Mortality rate was left as a free parameter. Loss to HTLs was derived from Chakraborty et al. (2017).

$$\mu = \frac{J_{tot}}{V} \tag{10}$$

Leakage of either carbon or nitrogen occurs when these are in excess inside the cell. Therefore, the leakage of carbon is

$$J_{Cleak} = \max[0, J_L - J_R - J_N] \tag{11}$$

and the leakage of N is the inverse of the carbon leakage:

$$J_{NLeak} = \max[0, -J_L + J_R + J_N] \tag{12}$$

Temperature dependencies

We consider temperature dependencies on carbon fixation, diffusive uptake, respiration, and biosynthetic processes. All dependencies are described by multiplying the processes with a Q_{10} factor, and therefore the rate R at a given temperature T becomes

$$R = R_{ref} Q_{10}^{(T - T_{ref})/10^{\circ}} \tag{13}$$

The reference rate R_{ref} is defined as the rate at temperature T_{ref} = 18°C (Table 1), and the value of Q_{10} represents the factorial increase when the temperature is increased by 10°C. We use the Q_{10} factor to describe temperature dependencies as this factor is much more intuitive than the Arrhenius equation and the corresponding activation energy. When Q_{10} = 1, there is no change with temperature; $Q_{10} > 1$ is an increase of a rate with temperature and the opposite effect for $Q_{10} < 1$. Recall that here we focus on the response of the overall community, which is the upper envelope of the temperature response of all species together (Eppley 1972; Edwards et al. 2016). Therefore, the shape of the community curve is not unimodal (as the species-specific response) but exponential within the range of temperatures where biological rates are functional. Carbon fixation at low light levels is temperature independent (Raven and Geider 1988; Clarke 2017); therefore, we use a Q_{10} = 1 for the light affinity α_L (Table 1). The

temperature dependency of nutrient affinity is governed by the temperature scaling of molecular diffusivity, which is proportional to viscosity. The viscosity of sea water doubles over a 20°C temperature increase from 2°C to 22°C, implying that diffusivity has $Q_{10} = 1.5$ approximately (Jumars et al. 1993; Thingstad and Aksnes 2019). Active encounters with prey are described by the clearance rate (Andersen et al. 2016). The clearance rate has a complicated response to temperature as it depends on the physical environment and the motility of the organisms. Consequently, the response might vary depending on whether the prey, the predator, or both are motile. Assuming the latter case, we could consider that encounter rates increase, also escape rates increase, with the approximate result that both effects cancel one another. In the absence of an empirically justified temperature scaling, we assume a $Q_{10} = 1$. Respiration and maximum potential growth rate scale with a Q_{10} close to 2 (Eppley 1972; Clarke 2003). Under resource limitation, all the temperature scalings are below 2, because respiration has a Q_{10} of 2. As the Q_{10} of respiration is larger than any resource-limited uptake process, the growth efficiency of a cell (anabolic processes – catabolic processes) decreases when resources are limiting (López-Urrutia and Morán 2007).

Bacteria

Bacteria are similar to the generalists, but they are smaller and they do not photosynthesize or engage in phagotrophy. Instead, they acquire N and dissolved organic carbon (DOC) by diffusive uptake, and so the functional responses for these resources are the same form as for nutrients in the generalist model (Eq. 3), with different affinity values for DOC (Table 1). Additionally, we assume that bacteria are able to hydrolyze particulate organic matter (POM), which is then transferred to the dissolved N and C pools. POM hydrolysis is represented by a saturating response (Anderson and Williams 1998):

$$J_{\mathrm{POM}} = \mu_{\mathrm{POM}} \frac{\alpha_{\mathrm{POM}} P}{\alpha_{\mathrm{POM}} P + \mu_{\mathrm{POM}}} \tag{14}$$

where P is the concentration of POM, μ_{POM} is the maximum specific hydrolysis rate of POM (μg C d^{-1} cell^{-1}), and α_{POM} is the initial slope of the functional response for hydrolysis (L d^{-1} cell^{-1}). The flux of the limiting resource determines the total biomass synthesis rate:

$$J_{\mathrm{tot}} = \min[J_{\mathrm{DOC}} - J_{\mathrm{R}}, J_{\mathrm{N}}]. \tag{15}$$

The specific division rate of the population is the same as in Eq. 10 and leakage of C and N as in Eqs. 11 and 12, replacing J_{L} by J_{DOC}.

Microbial community model

The generalist model is embedded in a biogeochemical food web with six main compartments (Fig. 2): bacteria (B), small generalist (G_1), large generalist (G_2), nitrogen (N), including both organic and inorganic, DOC (D), and POM (P), the latter including both nitrogen and carbon. Parameters and variables are listed in Table 1. The key structural elements are the two generalist groups. To allow adaptation of the composition and function of the generalists, we describe them as a system of

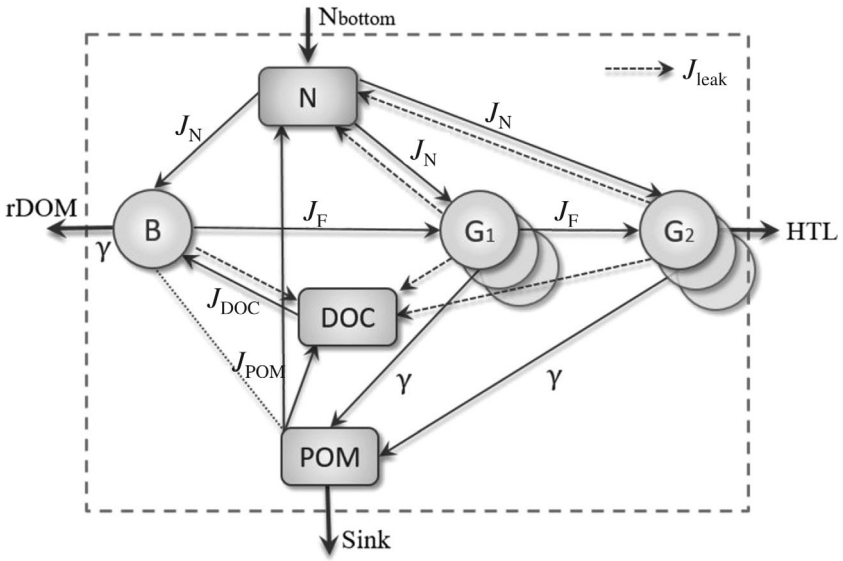

Fig. 2. Biological system of the microbial community. The system contains six carbon and nitrogen pools: bacteria (B), small generalists (G_1), large generalists (G_2), DOC, POM, and a dissolved nitrogen pool (N), which includes both organic and inorganic N. Fluxes (J) are explained in Microbial Community Model section. Dashed lines represent leakage of carbon and nitrogen. The pointed line in J_{POM} is the action of bacteria degrading POM which then goes to the N and DOC pools.

infinite diversity (Bruggeman and Kooijman 2007), i.e., as a distribution of biomass along the trait-axis φ_L.

The currency of the model is μg C L^{-1}, with the exception of the nitrogen pool, which is given in μg N L^{-1}, hence the conversion factor $Q_{C:N}$ in the corresponding equations. Pools containing both carbon and nitrogen possess the same stoichiometry, $Q_{C:N}$. All organisms take nutrients from the N pool, bacteria also rely on DOC and hydrolyse POM, which goes to the DOC pool and to nutrients. Generalists perform both photosynthesis and phagotrophy: small generalists eat bacteria (J_{F1}), and large generalists eat small generalists (J_{F2}). Natural mortality (γ) is represented by a quadratic term, allowing to impose a control when concentrations are too high. In the natural environment, such could represent viral lysis when prey density is high. Still the value of γ was taken small enough as not to rule model dynamics. A fraction δ of dead matter goes to the dissolved pools, and $(1-\delta)$ to the POM pool. Excess carbon and nitrogen in the cells is leaked (J_{Cleak} and J_{Nleak}, respectively), going to the corresponding dissolved pools. We assume that dead material from bacteria is refractory DOM, rDOM (Jiao et al. 2010), which is removed from the system due to its low turnover rate. The modeled system, its compartments, and fluxes are illustrated in Fig. 2, and the governing equations are

Physical setup

We used the Framework for Aquatic Biogeochemical Models (FABM; Bruggeman and Bolding 2014), which allow the coupling of custom biochemical models with different ocean models. Here, we used the 1D water column model General Ocean Turbulence Model (GOTM; Burchard et al. 1999). The model simulates the upper 50 m of a water column of a temperate region (seasonal). Physical data from the L4 station (50°N, 4°W; in the English Channel) was used as a model setup and later some modifications were introduced (we therefore did not intend to explicitly model the L4 station). For the L4 station water-column setup refer to the ERSEM (European Regional Seas Ecosystem Model) source codes (https://gitlab.ecosystem-modelling.pml.ac.uk/users/sign_in) explained in Butenschön et al. (2016). In our case, we set an open bottom boundary, allowing the entrance of nutrients and the export of detrital matter. The input rate of nutrients is defined as $V_{N,\ bottom} = \nu (N_b - N)$, where ν is the exchange rate equivalent to 1 d^{-1}, N_b a fixed concentration (140 μg N L^{-1}). Sinking POM leaves through the bottom boundary at a rate equivalent to the sinking velocity, set at 10 m d^{-1}. The simulation time was 9 yr, and by the end of the simulations, solutions had converged to a periodic solution. The FABM-GOTM code of the model can be found in https://github.com/cam-sp/Plankton-temperature-resources.

$$
\begin{aligned}
\frac{dG_{1,i}}{dt} &= \mu_{1,i}G_{1,i} - \gamma G_{1,i}^2 - \frac{G_{1,i}}{\sum_{i=1}^{n} G_{1,i}}\left(\sum_{j=1}^{n}\frac{J_{F.2,j}}{V_2}G_{2,j}\right)\\
\frac{dG_{2,i}}{dt} &= \mu_{2,i}G_{2,i} - \gamma G_{2,i}^2 - m_{htl}G_{2,i}\\
\frac{dB}{dt} &= \mu_B B - \gamma B^2 - \sum_{i=1}^{n}\frac{J_{F.1,i}G_{1,i}}{V_1}\\
\frac{dN}{dt} &= \frac{1}{Q_{C:N}}\left(-\sum_{i=1}^{n}\left(\frac{J_{N.1,i}}{V_1}G_{1,i} + \frac{J_{N.2,i}}{V_2}G_{2,i}\right) - \frac{J_{N.B}}{V_B}B\right.\\
&\quad \left. + \sum_{i=1}^{n}\left(\frac{J_{Nleak.1,i}}{V_1}G_{1,i} + \frac{J_{Nleak.2,i}}{V_2}G_{2,i}\right) + \frac{J_{Nleak.B}}{V_B}B + \frac{J_{POM}}{V_B}B + \delta\sum_{i=1}^{n}\gamma\left(G_{1,i}^2 + G_{2,i}^2\right)\right)\\
\frac{dP}{dt} &= (1-\delta)\sum_{i=1}^{n}\gamma\left(G_{1,i}^2 + G_{2,i}^2\right) - \frac{J_{POM}}{V_B}B\\
\frac{dD}{dt} &= \sum_{i=1}^{n}\left(\frac{J_{Cleak.1,i}}{V_1}G_{1,i} + \frac{J_{Cleak2,i}}{V_2}G_{2,i}\right) + \frac{J_{leak.B}}{V_B}B - \frac{J_{DOC}}{V_B}B + \frac{J_{POM}}{V_B}B + \delta\sum_{i=1}^{n}\gamma\left(G_{1,i}^2 + G_{2,i}^2\right)
\end{aligned}
\tag{16}
$$

The last term in the large generalist equation corresponds to losses to HTLs m_{HTL} (d^{-1}). The trait distributions of the two generalist groups are discretized with $n = 20$ trait groups representing cells with investments in light harvesting $\varphi_{L,}$ varying from 0 to 1/2 (and, correspondingly, investments in biosynthesis varying from 1/2 to 0).

As we seek to observe the direct effects of temperature on organisms (without the physical environment being altered), an increase in temperature was not forced in the physical environment itself but only in the biological system, so only biological processes are affected by the increase in temperature. We exposed the system to a +3°C rear in temperature, expecting a

linear response in ecosystem functions. Additionally, a 3°C increase falls within the estimated range of temperature rise due to climate change in the next 100 yr (Stocker et al. 2013).

Ecosystem function

As indicators of ecosystem function, we consider carbon flux into the ecosystem (gross primary production [GPP]), carbon cycling within the ecosystem (carbon transfer to HTLs), and carbon flux out of the ecosystem (respiration, carbon export, and rDOM production). GPP, the total amount of carbon fixed by photosynthesis, can be directed either to population growth if enough nutrients are available or leaked and transferred to the dissolved pool. Redistribution inside the ecosystem occurs through the net production to HTLs as the amount of carbon lost from the m_{HTL} term. The main losses are export to depth, as the flux of *POM* across 50 m, and the formation of refractory DOM, *rDOM*, through lysis of bacteria. We characterize the efficiencies of these fluxes as the ratio between them and GPP: the HTL efficiency ϵ_{HTL} as the ratio between losses and GPP ($\epsilon_{\mathrm{HTL}} = m_{\mathrm{HTL}} G_2/\mathrm{GPP}$). The ratio of respired to fixed carbon in the ecosystem (also referred to in the literature as metabolic balance) is $\epsilon_{\mathrm{resp}} = (J_{\mathrm{R,G_1}} + J_{\mathrm{R,G_2}} + J_{\mathrm{R,B}})/\mathrm{GPP}$, where values that surpass unity mean that the system is completely heterotrophic, i.e., more carbon is being respired than fixed, which can happen if there has been an accumulation of dissolved or POM over time. The export efficiency is the ratio between export flux at a given depth and integrated GPP over that depth horizon ($\epsilon_{\mathrm{C_{exp}}} = \mathrm{C_{exported}}/\mathrm{GPP}$). A higher $\epsilon_{\mathrm{C_{exp}}}$ indicates an ecosystem more effective in exporting carbon. Finally, the rDOM produced relative to GPP is $\epsilon_{\mathrm{rDOM}} = \gamma B^2/\mathrm{GPP}$, where higher values indicate a strengthening of the microbial loop and pump.

Results

We first perform a simple optimization analysis of the cell model to find the investments that maximize cell division rate under various resource and temperature combinations ("resources" include light). Next, we embed the cell model in the biological–physical model and explore the response of the system to a rise in temperature.

Optimization of the cell model

The optimal investment φ_{L}^{*} maximizes division rate (Eq.10) in an environment of light (L), nutrients (N), and food (F):

$$\varphi_{\mathrm{L}}^{*}(L,N,F) = \underset{\varphi_{\mathrm{L}}}{\mathrm{argmax}} \{\, \mu(\varphi_{\mathrm{L}};L,N,F) \,\} \tag{17}$$

By assuming that the plankton species with the highest division rate dominates a given environment, we can use the traits of the optimal cells as representatives of the overall community. Figure 3 shows the temperature response of division rate for the optimal cells, $\mu(\varphi_{\mathrm{L}}^{*};L,N,F)$. Depending on the environment, there are clear variations in the cells' investment in light harvesting vs. biomass synthesis and in their trophic strategy.

Investments in photo harvesting increases as light decreases when food availability is low (shaded areas in Fig. 3). In low light conditions, cells are light limited and will prioritize light harvesting by increasing investments in light uptake φ_{L}. Conversely, under high light, the cells are limited by their capacity to synthesize biomass (φ_{B}) and consequently lower their investment in φ_{L} to maximize their capacity for synthesis. When food is abundant, investments in photo harvesting stay constant across light gradients. In this case, cells are limited by nutrients, and therefore, light investments will be reduced as much as possible as to maximize synthesis. This reduction in light investments should however not make the cell carbon limited. All in all, investments are adjusted to lessen the constraint from the limiting process.

All cells are mixotrophic, but there are clear differences in the degree of mixotrophy between small and large cells (dashed lines in Fig. 3). Small cells are primarily autotrophic and obtain most of their carbon and nutrients from photo harvesting and nutrient uptake, while large cells get the majority of their resources from phagotrophy. Nevertheless, large cells are not purely heterotrophic; they do phototrophy to at least cover their respiratory costs. In that way, the large cells can use all the carbon and nutrients gained from phagotrophy for synthesis of new biomass. Still, larger cells invest less in light harvesting than small cells (*see* Chakraborty et al. 2017).

Exposing the cells to a rise in temperature elicits changed investments and division rates. First, investments in photo harvesting increase with temperature. This is a response to biosynthesis becoming faster with temperature ($Q_{10} = 2$), while photosynthesis does not ($Q_{10} = 1$). Therefore, increasing temperature shifts the limiting factor for growth from biosynthesis toward photo harvesting, everything else being equal.

Temperature response is highest in resource-unlimited conditions and weakest in resource-limited conditions, particularly under carbon (light and food) limitation (Fig. 4). The differences in temperature responses mainly reflect whether resource uptake or synthesis is limiting growth: response of the cell to temperature is small when resources are limiting, whereas when resources are under replete conditions the response increases to a $Q_{10} \approx 2$. To a lesser degree, the response is determined by the temperature response of the uptake pathway, because only nutrient uptake has a $Q_{10} > 1$. Large cells in general have slower division rates than small cells, which indicate that they are in general more limited by resource uptake than synthesis. It is possible for $Q_{10} < 1$ at low concentrations of carbon resources (light and food). This results from respiration increasing at a higher rate with temperature than resource uptakes at limiting conditions ($Q_{10} = 2$ for respiration vs. $Q_{10} = 1$ for affinity for food and light). And therefore, when resources are low, an increase in temperature results in a reduced growth, because the relative

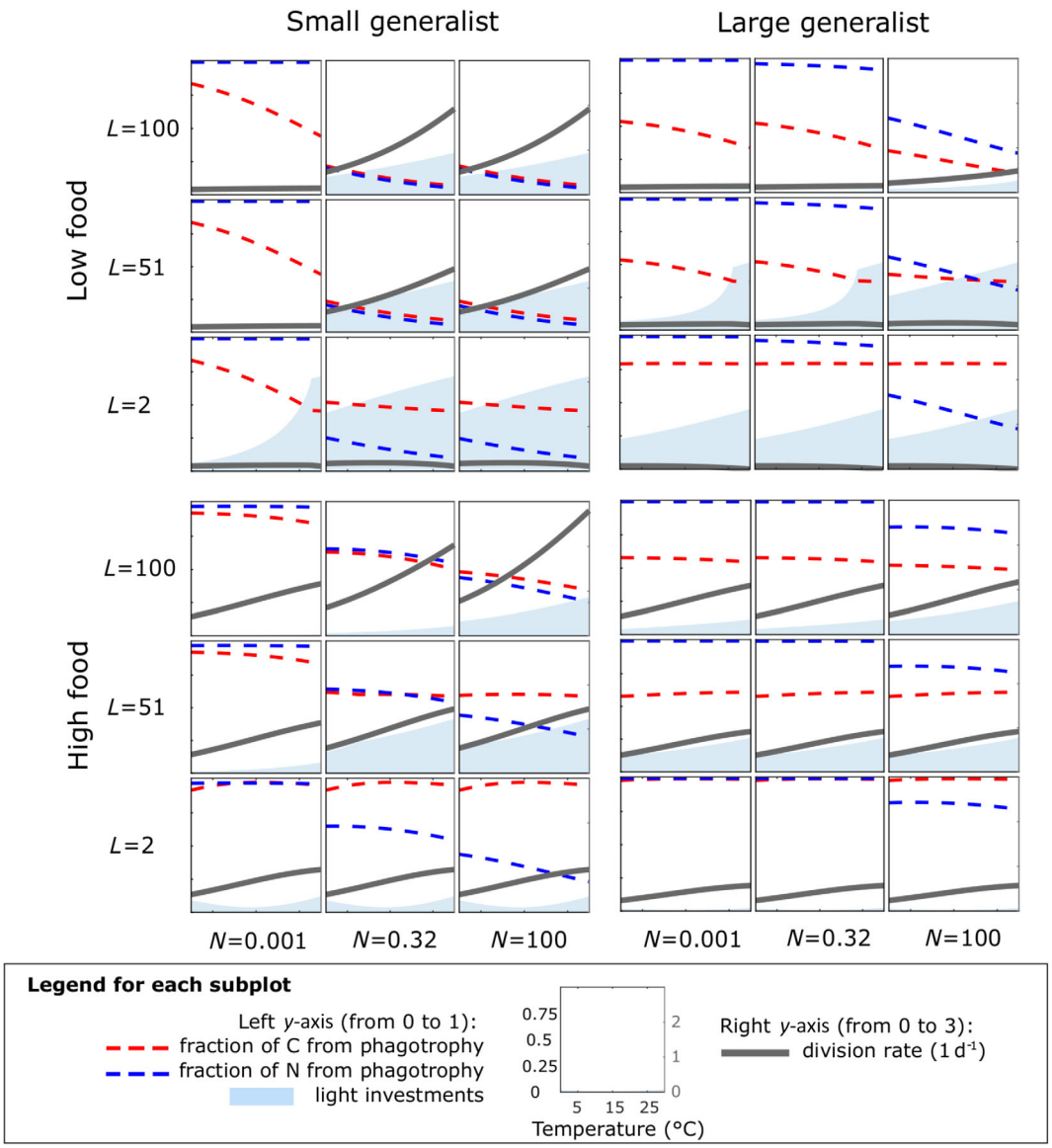

Fig. 3. Temperature dependency of division rate, light investments, and fraction of carbon and nutrients derived from phagotrophy for small and large generalists (left and right column, respectively) under various resource conditions. The upper bloc of panels is at low food levels (F = 5 μg C L^{-1}) and the lower at high food levels (F = 5 μg C L^{-1}). Each row of small panels is under a given condition of light (L in W m^{-2}) and each column a given concentration of nutrients (N in μg N L^{-1}). [Color figure can be viewed at wileyonlinelibrary.com]

loss of carbon due to respiration outweighs the relative gain in carbon fixation. This effect no longer applies when resource levels are higher as temperature has a greater effect on biosynthesis, which has the same Q_{10} as respiration, than on affinity. Overall, the temperature response of the optimal cells varies with the resource environment, being strongest under unlimited resources and weakest under limiting conditions.

Biological and physical model

The optimization analysis was made for fixed resource concentrations; however, in reality, resource concentrations change with time and depth (in particular light) and are emergent outcomes of competition and predation (nutrients and food). The resource environment will determine which process limits growth, and the limitation (carbon, nutrients, or biosynthesis) will ultimately shape the community's temperature response. We thus explore a dynamic resource environment in a temperate system. The following will focus on identifying the limiting process: carbon (photosynthesis), nutrients (nutrient uptake), or synthesis. Knowing the limiting process gives insight into the community temperature response.

The modeled seasonal succession well represents typical observed successions (Fig. 5): an early spring bloom of mainly phototrophic small cells is grazed by larger mainly

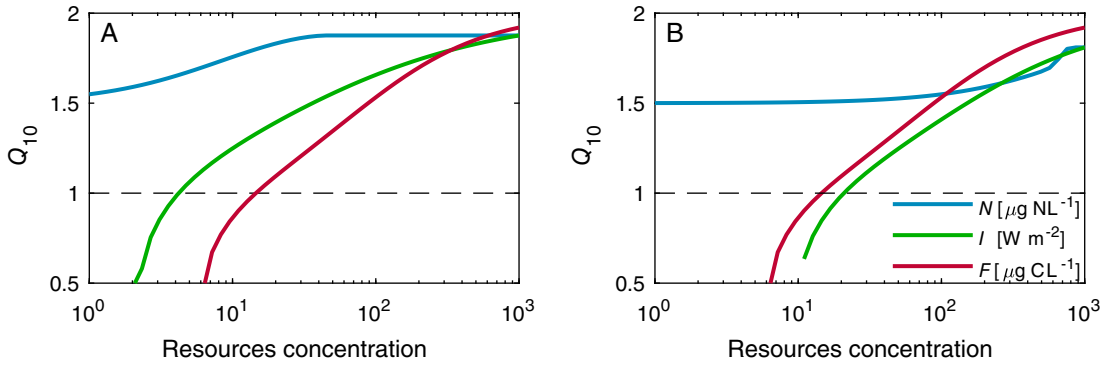

Fig. 4. Q_{10} values of the temperature response of cell division rate as a function of resource conditions, as determined by fits to the actual response (*see* Fig. 3) for G_1 (**A**) and G_2 (**B**). The *x*-axis represents changes in light (W m^{-2}), nutrients (μg N L^{-1}), and food (μg C L^{-1}), from 0 to 1000. To plot the nitrogen (*N*) curve, we fixed the values for light and food (I = 1000, F = 0). For the light curve (*I*), we fixed N = 1000 and F = 0. Finally, for the food curve *F*, both light and nutrients were fixed to 0. The Q_{10} was fitted for the optimal growth obtained for each condition; therefore, investments might also be different. Only effects on positive growth are shown. The Q_{10} for each combination of light, food, and nutrients was calculated by linear regression between temperature and log of the growth rate. [Color figure can be viewed at wileyonlinelibrary.com]

phagotrophic cells. The summer production is limited in the upper mixed layer. A small autumn bloom is triggered by inorganic nitrogen mixed up from the deeper layer. The small cells are predominantly phototrophic, although they still obtain up to 30% of their carbon from food. The larger cells change their trophic strategy throughout the season. In the early summer, they are mainly heterotrophic, feeding on the smaller cells, while in the summer, they become increasingly mixotrophic. Phagotrophy is the main source of nutrients during summer for both small and large cells.

The optimization model showed how the temperature response of cells is largely determined by whether the limiting factor is resource uptake (weak response) or synthesis (strong response) (Fig. 3). In the dynamic environment, the small generalists are predominantly limited by carbon (light), except in the late summer where they are nutrient limited and their growth rate is low (Fig. 5). As synthesis has the highest Q_{10}, we expect that the small cells will show a strong response to increasing temperatures, as they tend to be less limited by resources (Fig. 6). Conversely, large generalists are predominantly limited by resources, and their growth is not controlled by the biosynthetic rate, due to their need for much larger resources concentrations (Fig. 4). In summary, we expect smaller cells to have a stronger temperature response than larger cells.

How the division rate changes with temperature is only one part of understanding how a community responds to temperature changes. Other important factors are changes in resource availability (prey) and predation rates. Figure 7 shows water column integrated dynamical variables over a seasonal cycle in the base-line scenario and in a scenario in which temperature was raised +3°C, illustrating how temperature changes biomass and resulting resource availability. As suggested by the analysis of limitation above, the small generalists responds positively to the temperature increase, while overall the biomass of the larger cells remain largely unchanged. However, the overall picture is more nuanced. Increased carbon leakage increases DOC to the benefit of the bacteria population leading to increased overall bacteria respiration. Further, at higher temperature, cells are able to drive nutrients to lower concentrations enabling a higher net primary production.

The overall functions of the ecosystem in terms of its yearly carbon budget are shown in Fig. 8. The system fixes about 80 g C m^{-2} yr^{-1}. Most is lost as refractory DOM and respiration, and only about 3 g C are exported as particulate carbon, either to the deep ocean or to HTLs. The average response of these fluxes to the 3°C temperature increase is an increase of about 20%, corresponding to a Q_{10} of about 1.8. The responses of the ecosystem efficiencies are more modest, with a lower fraction of GPP being exported ($Q_{10} \approx 1.5$), unchanged efficiency of DOM production and trophic transfer, and an increased fraction of GPP being respired ($Q_{10} \approx 1.4$). All in all, in absolute terms, all rates increase, yet, in relative terms, we have a more heterotrophic system (higher metabolic balance) and a system less efficient at exporting carbon to depth.

Discussion

We have developed a trait-based model of the temperature dependency of the primary mass flows in a pelagic protist community. The model is mechanistic and based on temperature responses of fundamental processes and on general rules for how resource uptakes scale with cell size. There is a growing realization of the need for a better representation of the temperature dependence of primary producers in the ocean, and in particular, the need to understand how these temperature dependencies are tempered by the availability of various resources (Schaum et al. 2017; Thomas et al. 2017; Marañón et al. 2018). The trait-based formulation of our model makes it possible to go beyond the responses of single

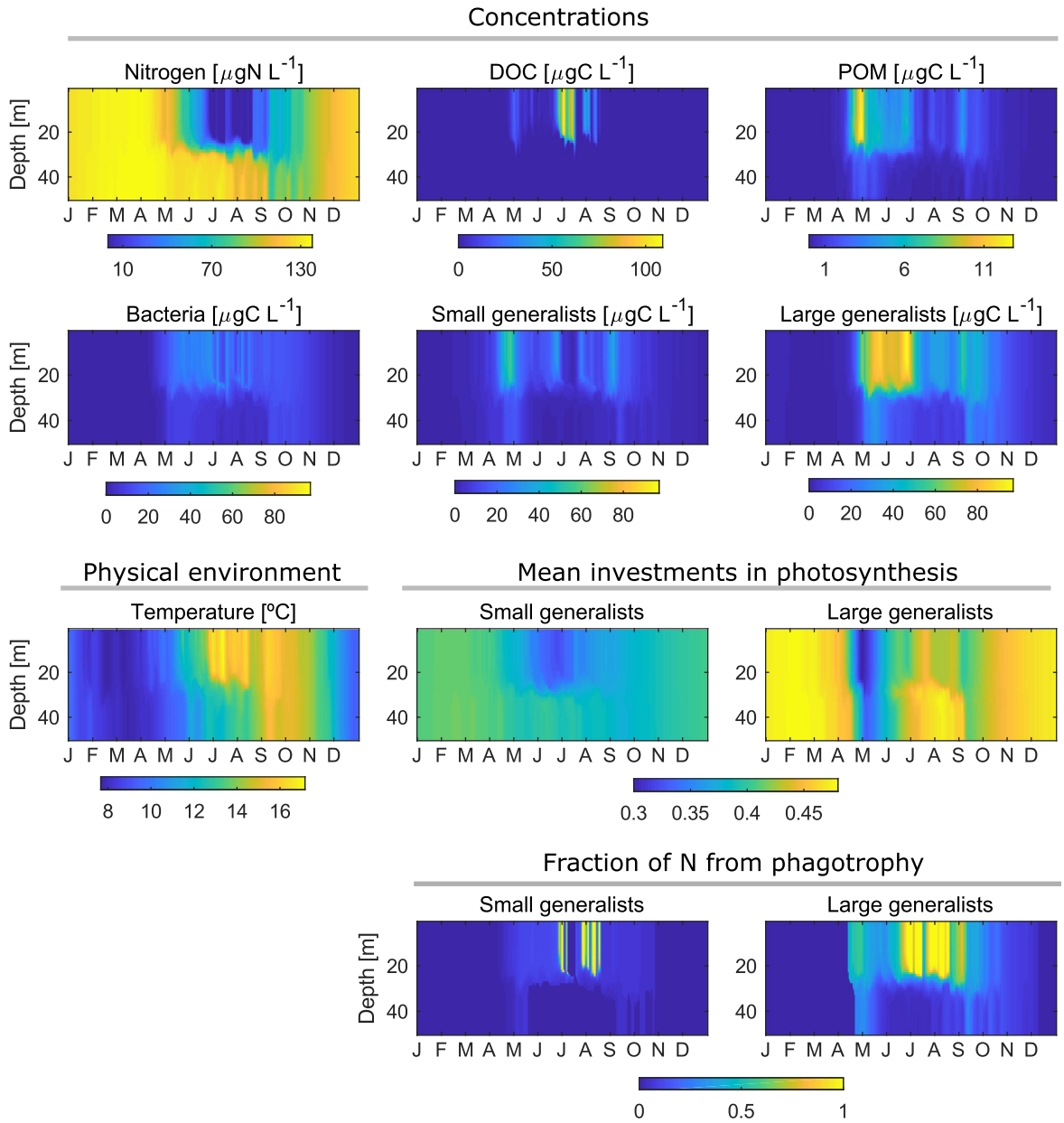

Fig. 5. Seasonal succession in a temperate water column. Note varying ranges on the concentrations of carbon. Mean investments are calculated as biomass weighted mean: $\overline{\varphi_L} = \sum_i \varphi_{L,i} B_i / n$, where $n = 20$ is the number of trait groups. The two lowest panels show the relative gains of nutrients coming from phagotrophy ($J_F : J_N$). [Color figure can be viewed at wileyonlinelibrary.com]

cells and to simulate how an entire community adapts to environmental conditions of light, nutrients, food, and temperature. As an example, we have simulated the seasonal succession in a temperate system and its response to a temperature increase. Despite the conceptual simplicity of the model, the community response to a temperature increase is complex.

The temperature response of the cells depends upon which process is limiting. Limitation by biosynthesis leads to a strong temperature response, while resource limitation leads to weak temperature responses. On the level of individual cells, we find that small cells are typically limited by their ability to perform biosynthesis, while larger cells are limited by resource uptake. This difference makes small cells more sensitive to changes in temperature than large cells, as the biosynthesis rate changes faster with temperature than resource uptake rates. This low-temperature response under nutrient limitation has also been observed experimentally (Marañón et al. 2018) and in meta-analysis (Thomas et al. 2017). Others observed different effects of temperature depending on whether the system was bottom-up or top-down controlled (Chen et al. 2012; Peter and Sommer 2013; Morán et al.

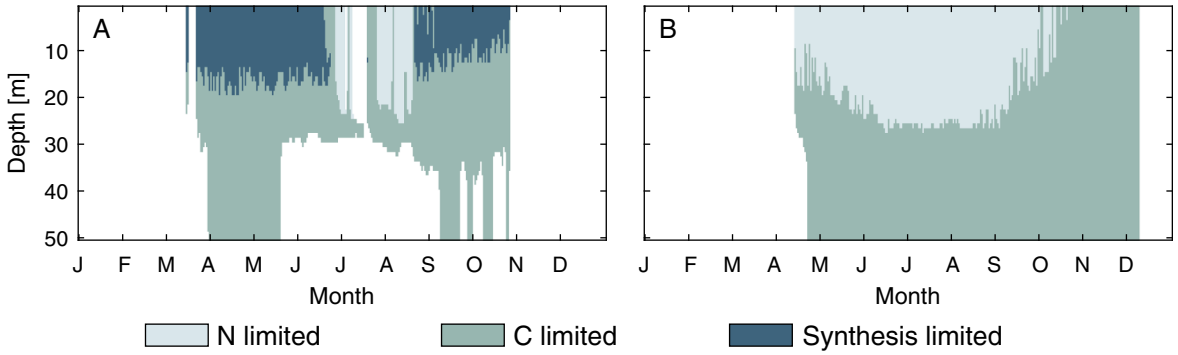

Fig. 6. Illustration of the limiting process for small (**A**) and large generalists (**B**). We only considered the trait group with the highest biomass at each time and depth. The colors show whether growth rate is ruled by biosynthetic rate or by uptake of resources, and in the latter case, whether they are limited by carbon or nitrogen. Carbon limitation occurs if leaks of nitrogen overcome carbon leaks, and the other way around for N limitation. Synthesis limitation occurs where mean (limiting resources/K) is larger than 1, being K the half saturation constant for that given resource and equivalent to M/A_X. White regions indicate biomass concentrations below 5 μg C L^{-1}. [Color figure can be viewed at wileyonlinelibrary.com]

2017), and López-Urrutia and Morán (2007) observed a decrease in bacterial growth efficiency with temperature when resource limited. Here, we show that not only does nutrient limitation plays a role but any resource uptake limitation will tend to weaken the temperature responses. We observe a broad range of temperature response, from flat (no response) toward a Q_{10} of around 2, depending on the degree of resources limitation. Light limitation in particular will give a particularly weak response due to photosynthesis at nonsaturating levels of light being temperature independent (Raven and Geider 1988; Clarke 2019).

The insight regarding the key role of resource limitation was made possible by explicitly separating the process of assimilation and synthesis in the functional response in the model. If these two processes are considered together, the role of limitation becomes opaque. For instance, functional responses are usually formulated with the half-saturation constant, which is the ratio between maximum uptake and substrate affinity. Hence, this formulation mixes the processes of assimilation and enzymatic activity, which makes it unsuitable for mechanistically describing the limiting process and temperature responses (*see* Thingstad and Aksnes 2019).

When cells are exposed to resource competition in a water column, they drive down the concentration of the limiting resource (except light for which they do not compete appreciably). The lowered resource concentration leads to resource limitation and thereby weak temperature responses. The example we used to explore resource competition was of a

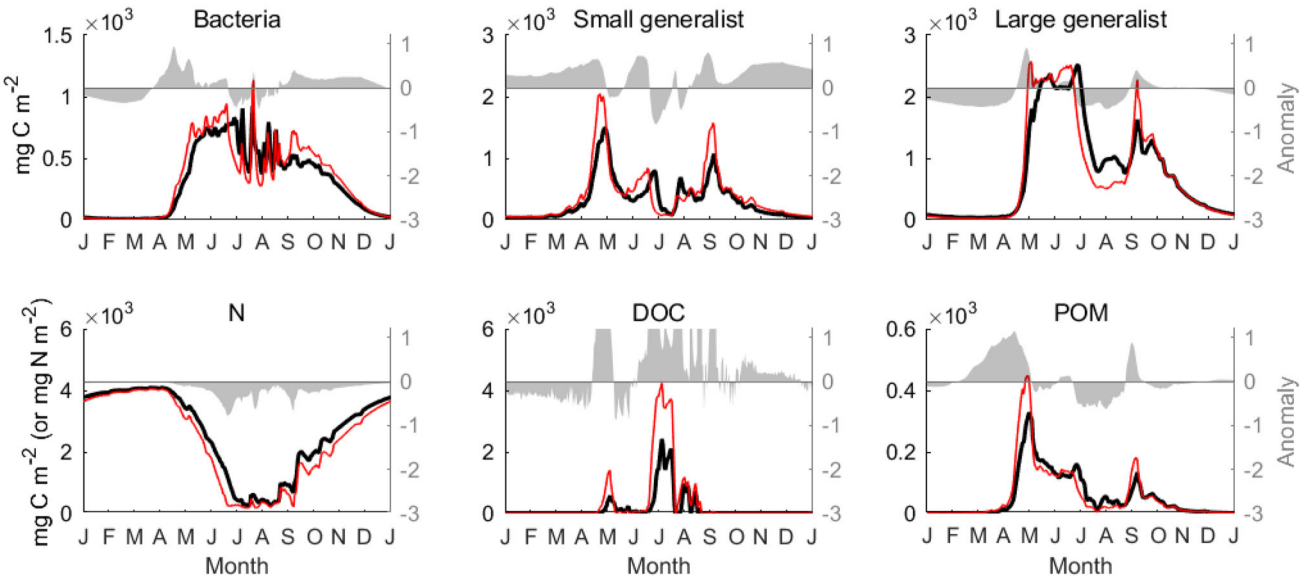

Fig. 7. Dynamical variables integrated over the upper 30 m of the water column. Black line is the base-line scenario, red is the +3°C scenario (left y-axis). Everything is in units of mg C m^{-2}, except the nitrogen pool which is in mg N m^{-2}. Upper shaded areas are the fraction of concentration changed relative to the base-line scenario (right y-axis), negative values mean a decrease while positive an increase. The high anomaly values in the DOC plot are an artifact of the rapid change in DOC concentration over time and have therefore been left out. [Color figure can be viewed at wileyonlinelibrary.com]

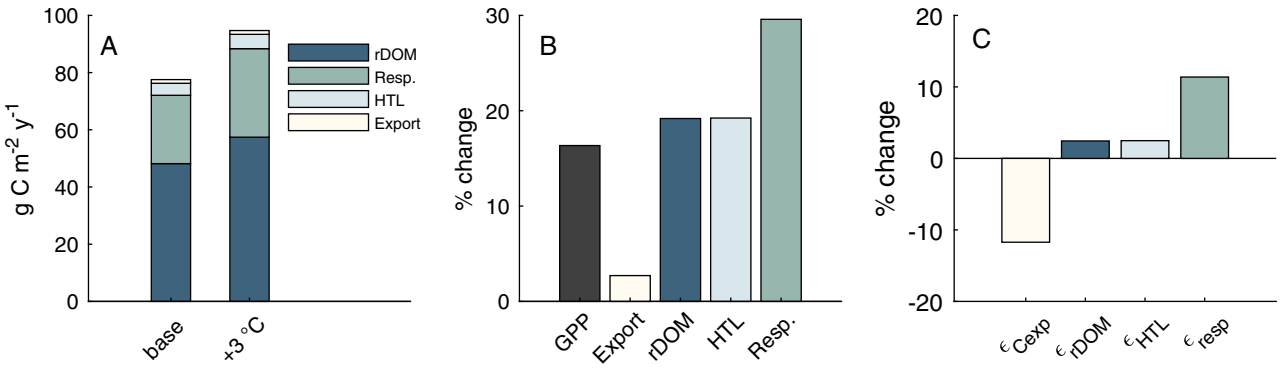

Fig. 8. Ecosystem functions and their response to a 3°C increase in temperature. Panel **A** shows total GPP over a year and its further fate. The functions are: GPP, production of rDOM, respiration, losses to export, and losses to HTLs. Panel **B** shows the total change in percent for each rate in response to the 3°C increase in temperature. Panel **C** shows the percent change relative to GPP in response to the temperature increase. Carbon flows relative to GPP are: export efficiency ($\epsilon_{Cexp} = C_{exported}/GPP$), rDOM production efficiency ($\epsilon_{rDOM} = \gamma B^2/GPP$), trophic transfer efficiency ($\epsilon_{HTL} = m_{HTL}G_2/GPP$), and respiration ($\epsilon_{resp} = (J_{R,G_1} + J_{R,G_2} + J_{R,B})/GPP$). [Color figure can be viewed at wileyonlinelibrary.com]

temperate seasonal succession. In this example, the early bloom period will not be resource limited, while the summer is. If we instead consider a low-latitude oligotrophic ocean, resource limitation will be stronger throughout the year, and we expect the temperature response to be even weaker. In any case, the diversity of temperature responses makes it difficult to apply a single Q_{10} or Arrhenius temperature function to protist growth rates in ecosystem models. Even assuming differential temperature effects between autotrophs and heterotrophs (Brown et al. 2004) is insufficient (Chen and Laws 2017).

Measures of ecosystem function increase overall with a Q_{10} around 1.8; a warmer ocean fixes more carbon, creates more DOM and rDOM, sends more carbon to HTLs, and respires more carbon. Nevertheless, the warmer ecosystem is less efficient at retaining carbon, as more of it is respired. We also find a negative relationship between ef-ratio (export relative to GPP) and temperature, in agreement with the literature (Pomeroy and Deibel 1986; Laws et al. 2000, 2011; Cael and Follows 2016; Cael et al. 2017). There is a reduction in relative cell size of the community, due to higher competition for nutrients during the stratified period (even without the thermal effect on water column stability), and the better performance of bacteria due to higher biosynthetic rate and DOC concentrations. Overall, there is an enhancement in the importance of the microbial loop and the microbial pump.

The model is based on simplifications, particularly in the values of Q_{10}, in the role of DOM, in the choice of a fixed stoichiometry, and in the physics. Regarding Q_{10}, more knowledge is needed on the temperature of predator–prey interactions and the uptake of dissolved compounds. If, for example, the Q_{10} of predator–prey interaction is larger than 1, the overall community Q_{10} will increase. Production and degradation of DOM (labile, semilabile, refractory DOM, etc.) are sketchily represented. An example is the production of refractory DOM, which we assume is created by viral lysis of bacteria, represented by a quadratic mortality. The assumption of fixed stoichiometry is a rough simplification, particularly in autotrophs, which have variable C : N : P ratios due to luxury uptake (Droop 1974), and to differing investments in chloroplast, ribosomes, and cell walls in response to resource conditions (Toseland et al. 2013). As temperature affects competition for resources and investments in biosynthesis, it will also affect stoichiometry and thus macronutrients cycling prediction under climate change scenarios (Yvon-Durocher et al. 2017). We have now resolved the direct effects of temperature on organisms and the overall community, but left open the question of the relative strength of indirect (effects due to changes in the physical environment) vs. direct effects of climate change on the planktonic community. Overall, incorporation of the considerations previously mentioned will refine the results; however, they are not expected to fundamentally alter the general conclusion that the community-level temperature response is smaller than expected from metabolic considerations.

Conclusion

Effects of temperature on physiological processes have been studied for over a century, nevertheless, we argue that interpretation of data related to global warming could have been mislead by effects of resource limitation (López-Urrutia and Morán 2007; Behrenfeld et al. 2016). Here, by explicitly representing effects of temperature on processes responsible for growth in a mechanistic model, we show that patterns in the individual level can be scaled to observed trends in the ecosystem level and that species interactions can actually exacerbate nutrient limitation by increasing competition just by temperature effects per se. We anticipate an strengthening of the microbial activity and the increasing importance of the dissolved pathway and the microbial pump for carbon sequestration in the oceans, at least when it comes to direct effects of temperature in the microbial food web.

References

Allen, A., J. Gillooly, and J. Brown. 2005. Linking the global carbon cycle to individual metabolism. Funct. Ecol. **19**: 202–213. doi:10.1111/j.1365-2435.2005.00952.x

Andersen, K. H., and others. 2016. Characteristic sizes of life in the oceans, from bacteria to whales. Annu. Rev. Mar. Sci. **8**: 217–241. doi:10.1146/annurev-marine-122414-034144

Anderson, T., and P. l. B. Williams. 1998. Modelling the seasonal cycle of dissolved organic carbon at station e1 in the English Channel. Estuar. Coast. Shelf Sci. **46**: 93–109. doi:10.1006/ecss.1997.0257

Behrenfeld, M. J., and others. 2006. Climate-driven trends in contemporary ocean productivity. Nature **444**: 752–755. doi:10.1038/nature05317

Behrenfeld, M. J., and others. 2016. Revaluating Ocean warming impacts on global phytoplankton. Nat. Clim. Chang. **6**: 323–330. doi:10.1038/nclimate2838

Brown, J. H., J. F. Gillooly, A. P. Allen, V. M. Savage, and G. B. West. 2004. Toward a metabolic theory of ecology. Ecology **85**: 1771–1789. doi:10.1890/03-9000

Bruggeman, J., and S. Kooijman. 2007. A biodiversity-inspired approach to aquatic ecosystem modeling. Limnol. Oceanogr. **52**: 1533–1544. doi:10.4319/lo.2007.52.4.1533

Bruggeman, J., and K. Bolding. 2014. A general framework for aquatic biogeochemical models. Environ. Model Softw. **61**: 249–265. doi:10.1016/j.envsoft.2014.04.002

Burchard, H., K. Bolding, and M. R. Villarreal. 1999. GOTM, a general ocean turbulence model: Theory, implementation and test cases. Technical report EUR 18745. Space Applications Institute.

Butenschön, M., and others. 2016. Ersem 15.06: A generic model for marine biogeochemistry and the ecosystem dynamics of the lower trophic levels. Geosci. Model Dev. **9**: 1293–1339. doi:10.5194/gmd-9-1293-2016

Cael, B. B., and M. J. Follows. 2016. On the temperature dependence of oceanic export efficiency. Geophys. Res. Lett. **43**: 5170–5175. doi:10.1002/2016GL068877

Cael, B. B., K. Bisson, and M. J. Follows. 2017. How have recent temperature changes affected the efficiency of ocean biological carbon export? Limnol. Oceanogr. Lett. **2**: 113–118. doi:10.1002/lol2.10042

Chakraborty, S., L. T. Nielsen, and K. H. Andersen. 2017. Trophic strategies of unicellular plankton. Am. Nat. **189**: E77–E90. doi:10.1086/690764

Chen, B., M. R. Landry, B. Huang, and H. Liu. 2012. Does warming enhance the effect of microzooplankton grazing on marine phytoplankton in the ocean? Limnol. Oceanogr. **57**: 519–526. doi:10.4319/lo.2012.57.2.0519

Chen, B., and E. A. Laws. 2017. Is there a difference of temperature sensitivity between marine phytoplankton and heterotrophs? Limnol. Oceanogr. **62**: 806–817. doi:10.1002/lno.10462

Clarke, A. 2003. Costs and consequences of evolutionary temperature adaptation. Trends Ecol. Evol. **18**: 573–581. doi:10.1016/j.tree.2003.08.007

Clarke, A. 2017. Principles of thermal ecology: Temperature, energy, and life. Oxford Univ. Press. doi:10.1093/oso/9780199551668.001.0001

Daines, S. J., J. R. Clark, and T. M. Lenton. 2014. Multiple environmental controls on phytoplankton growth strategies determine adaptive responses of the N : P ratio. Ecol. Lett. **17**: 414–425. doi:10.1111/ele.12239

Doney, S. C. 2006. Oceanography: Plankton in a warmer world. Nature **444**: 695–696. doi:10.1038/444695a

Droop, M. 1974. The nutrient status of algal cells in continuous culture. J. Mar. Biol. Assoc. U. K. **54**: 825–855. doi:10.1017/S002531540005760X

Dutkiewicz, S., J. R. Scott, and M. Follows. 2013. Winners and losers: Ecological and biogeochemical changes in a warming ocean. Glob. Biogeochem. Cycles **27**: 463–477. doi:10.1002/gbc.20042

Edwards, K. F., M. K. Thomas, C. A. Klausmeier, and E. Litchman. 2016. Phytoplankton growth and the interaction of light and temperature: A synthesis at the species and community level. Limnol. Oceanogr. **61**: 1232–1244. doi:10.1002/lno.10282

Eppley, R. W. 1972. Temperature and phytoplankton growth in the sea. Fish. Bull. **70**: 1063–1085.

Jiao, N., and others. 2010. Microbial production of recalcitrant dissolved organic matter: Long-term carbon storage in the global ocean. Nat. Rev. Microbiol. **8**: 593–599. doi:10.1038/nrmicro2386

Jumars, P. A., J. W. Deming, P. S. Hill, L. Karp-Boss, P. L. Yager, and W. B. Dade. 1993. Physical constraints on marine osmotrophy in an optimal foraging context. Aquat. Microb. Ecol. **7**: 121–159.

Kahru, M., V. Brotas, M. Manzano-Sarabia, and B. Mitchell. 2011. Are phytoplankton blooms occurring earlier in the arctic? Glob. Chang. Biol. **17**: 1733–1739. doi:10.1111/j.1365-2486.2010.02312.x

Kiørboe, T. 2008. A mechanistic approach to plankton ecology. Princeton Univ. Press.

Kiørboe, T. 2011. How zooplankton feed: Mechanisms, traits and trade-offs. Biol. Rev. **86**: 311–339. doi:10.1111/j.1469-185X.2010.00148.x

Kiørboe, T., and A. G. Hirst. 2014. Shifts in mass scaling of respiration, feeding, and growth rates across life-form transitions in marine pelagic organisms. Am. Nat. **183**: E118–E130. doi:10.1086/675241

Laws, E. A., P. G. Falkowski, W. O. Smith, H. Ducklow, and J. J. McCarthy. 2000. Temperature effects on export production in the open ocean. Glob. Biogeochem. Cycles **14**: 1231–1246. doi:10.1029/1999GB001229

Laws, E. A., E. D'Sa, and P. Naik. 2011. Simple equations to estimate ratios of new or export production to total production from satellite-derived estimates of sea surface

temperature and primary production. Limnol. Oceanogr. Methods **9**: 593–601. doi:10.4319/lom.2011.9.593

López-Urrutia, Á., and X. A. G. Morán. 2007. Resource limitation of bacterial production distorts the temperature dependence of oceanic carbon cycling. Ecology **88**: 817–822. doi:10.1890/06-1641

Marañón, E., M. P. Lorenzo, P. Cermeño, and B. Mouriño-Carballido. 2018. Nutrient limitation suppresses the temperature dependence of phytoplankton metabolic rates. ISME J. **12**: 1836–1845. doi:10.1038/s41396-018-0105-1

Monod, J. 1949. The growth of bacterial cultures. Annu. Rev. Microbiol. **3**: 371–394. doi:10.1146/annurev.mi.03.100149.002103

Morán, X. A. G., J. M. Gasol, M. C. Pernice, J.-F. Mangot, R. Massana, E. Lara, D. Vaqué, and C. M. Duarte. 2017. Temperature regulation of marine heterotrophic prokaryotes increases latitudinally as a breach between bottom-up and top-down controls. Glob. Chang. Biol. **23**: 3956–3964. doi:10.1111/gcb.13730

Morán, X. A. G., A. Calvo-Díaz, N. Arandia-Gorostidi, and T. M. Huete-Stauffer. 2018. Temperature sensitivities of microbial plankton net growth rates are seasonally coherent and linked to nutrient availability. Environ. Microbiol. **20**: 3798–3810. doi:10.1111/1462-2920.14393

Munk, W., and G. Riley. 1952. Absorption of nutrients by aquatic plants. J. Mar. Res. **11**: 40.

Peter, K. H., and U. Sommer. 2013. Phytoplankton cell size reduction in response to warming mediated by nutrient limitation. PLoS One **8**: e71528. doi:10.1371/journal.pone.0071528

Pomeroy, L. R., and D. Deibel. 1986. Temperature regulation of bacterial activity during the spring bloom in newfoundland coastal waters. Science **233**: 359–361. doi:10.1126/science.233.4761.359

Raven, J. A., and R. J. Geider. 1988. Temperature and algal growth. New Phytol. **110**: 441–461. doi:10.1111/j.1469-8137.1988.tb00282.x

Schaum, C.-E., and others. 2017. Adaptation of phytoplankton to a decade of experimental warming linked to increased photosynthesis. Nat. Ecol. Evol. **1**: 0094. doi:10.1038/s41559-017-0094

Shuter, B. 1979. A model of physiological adaptation in unicellular algae. J. Theor. Biol. **78**: 519–552. doi:10.1016/0022-5193(79)90189-9

Sommer, U., K. H. Peter, S. Genitsaris, and M. Moustaka-Gouni. 2017. Do marine phytoplankton follow bergmann's rule sensu lato? Biol. Rev. **92**: 1011–1026. doi:10.1111/brv.12266

Stocker, T. F., and others. 2013. Climate change 2013: The physical science basis. Intergovernmental Panel on Climate Change, Working Group I Contribution to the IPCC Fifth Assessment Report (AR5). Cambridge Univ. Press.

Thingstad, T. F., and others. 2007. Ability of a minimum microbial food web model to reproduce response patterns observed in mesocosms manipulated with n and p, glucose, and si. J. Mar. Syst. **64**: 15–34. doi:10.1016/j.jmarsys.2006.02.009

Thingstad, T. F., and D. L. Aksnes. 2019. Why growth of nutrient-limited micro-organisms should have low-temperature sensitivity. ISME J. **13**: 557. doi:10.1038/s41396-018-0271-1

Thomas, M. K., C. T. Kremer, C. A. Klausmeier, and E. Litchman. 2012. A global pattern of thermal adaptation in marine phytoplankton. Science **338**: 1085–1088. doi:10.1126/science.1224836

Thomas, M. K., M. Aranguren-Gassis, C. T. Kremer, M. R. Gould, K. Anderson, C. A. Klausmeier, and E. Litchman. 2017. Temperature–nutrient interactions exacerbate sensitivity to warming in phytoplankton. Glob. Chang. Biol. **23**: 3269–3280. doi:10.1111/gcb.13641

Toseland, A., and others. 2013. The impact of temperature on marine phytoplankton resource allocation and metabolism. Nat. Clim. Chang. **3**: 979–984. doi:10.1038/nclimate1989

Yvon-Durocher, G., C.-E. Schaum, and M. Trimmer. 2017. The temperature dependence of phytoplankton stoichiometry: Investigating the roles of species sorting and local adaptation. Front. Microbiol. **8**: 2003. doi:10.3389/fmicb.2017.02003

Acknowledgments

A. W. Visser, K. H. Andersen, and C. Serra-Pompei acknowledge support from the Gordon & Betty Moore Foundation through award 5479 and the Centre for Ocean Life, a Villum Kahn Rasmussen Centre of Excellence funded by the Villum Foundation. G. I. Hagstrom acknowledges support from the Simons Foundation grant 395890, NSF award OCE-1848576, and the Centre for Ocean Life at DTU Aqua.

Conflict of Interest

None declared.

Submitted 08 October 2018
Revised 16 January 2019
Accepted 17 January 2019

Associate editor: Susanne Menden-Deuer